Investigation of superelastic electron scattering by laser-excited Ba. Experimental procedures and results

D. F. Register* and S. Trajmar
California Institute of Technology, Jet Propulsion Laboratory, 4800 Oak Grove Drive, Pasadena, California 91109

G. Csanak†
154 Cold Spring Road, No. 67, Stamford, Connecticut 06905

S. W. Jensen‡
Department of Physics, University of California, Riverside, Riverside, California 92521

M. A. Fineman
Department of Astronomy and Physics, Lycoming College, Williamsport, Pennsylvania 17701

R. T. Poe
Department of Physics, University of California, Riverside, Riverside, California 92521
(Received 17 January 1983)

Differential (in angle) electron scattering experiments on laser-excited ^{138}Ba ^1P were carried out at 30- and 100-eV impact energies. The laser light was linearly polarized and located in the scattering plane. The superelastic scattering signal was measured as a function of polarization direction of the laser light with respect to the scattering plane. It was found at low electron scattering angles that the superelastic scattering signal was asymmetric to reflection of the polarization vector with respect to the scattering plane. This is in contradiction with theoretical predictions. An attempt was made to pinpoint the reason for this observation, and a detailed investigation of the influence of experimental conditions on the superelastic scattering was undertaken. No explanation for the asymmetry has as yet been found.

I. INTRODUCTION

In recent years, a number of coherence studies of electron-atom collision processes have been carried out. Most of these measurements have used electron-photon coincidence techniques.[1] However, the same, and in some cases more, information can be obtained by studying superelastic electron scattering by laser-excited atoms.[2] This latter approach has been applied to Na by Hertel and Stoll[2] and to Ba by us.[3] These studies go beyond conventional electron collision cross-section measurements and yield detailed information about the properties (orientation and alignment parameters) of the excited atomic state prepared by the inverse (inelastic) electron impact process.[4,5]

A general theory for the interpretation of superelastic electron scattering by laser-excited atoms was developed by Macek and Hertel[4] based on the formalism of Fano and Macek.[5] A description of this theory, its extension to heavy elements, and its application to the present observations is given elsewhere.[6] In the case of superelastic scattering by Na (Ref. 7) (and also until recently in all electron-photon coincidence measurements), the Percival-Seaton hypothesis[8] of decoupling of spin and angular momenta during the collision was assumed. Recently it has been pointed out by Blum *et al.*[9] and Paixão *et al.*[10] that electron spin-orbit coupling has to be considered in general and the J,M_J coupling scheme has to be used to describe the target atom in its interaction with the continuum electron. This spin-orbit coupling causes the loss of reflection symmetry of the $M_J=1$ and $M_J=-1$ *scattering amplitudes* with respect to the scattering plane [in the case of a $(J=0)\rightarrow(J=1)$ excitation] and requires the introduction of two new source parameters, (ϵ,Δ) in addition to the three parameters (σ,Λ,χ) conventionally used in the LS coupling scheme. (In the latter case ϵ and Δ are zero). Nuclear-spin decoupling seems to be justified in electron scattering experiments.

In our studies concerning superelastic electron scattering by laser-excited ^{138}Ba $6s\,6p\ ^1P$ atoms, a *linearly polarized laser beam, located in the scattering plane* was utilized and the superelastic scattering intensity (I^S) was measured as a function of laser beam polarization angle (ψ) with respect to the scattering plane at fixed impact energies (E_o), electron scattering angles (θ_e), and laser beam directions (θ_v).[3] No spin selection was made in the incoming and scattered electrons. These measurements clearly indicate that Ba has to be described in the J,M_J coupling scheme. The experiments also showed a high degree of coherence between the $M_J=1$ and $M_J=-1$ scattering amplitudes and a much lower degree of coherence was observed for the $M_J=0$ and $M_J=\pm1$ amplitudes.[3(c)] It should be noted that in the previous evaluation of the experimental data,[3(c)] the low-angle asymmetry was not considered.

The Ba experiments also indicated that the reflection symmetry of the superelastic *scattering intensity* with respect to the scattering plane is lost at low scattering angles. The subject of the present paper is to describe in some detail the experimental arrangements and procedures, the results, and the investigations aimed at finding the possible cause of the observed asymmetry. Due to

the unexpected nature of this observation, the experiments are described in greater detail than normal. In a planned subsequent paper,[6] we will derive the analytical expressions necessary for the interpretation of the superelastic scattering results and discuss the present data in terms of this theory.

II. APPARATUS, TECHNIQUES, AND SCATTERING GEOMETRY

The electron impact spectrometer used in the present study has been described in some detail elsewhere.[3(a)] The electron gun consisted of two cylindrical electrostatic lens systems (one for producing the low-energy collimated beam for the energy selector and one for focusing the energy selected beam with the required impact energy, into the scattering region) and two tandem hemispherical energy selectors. Typical beam current at the scattering center was about 20 nA with about 0.080 eV energy width [full width at half maximum (FWHM)] and 0.13 cm diameter (with about $\pm 1°$ divergence). In the present experiments the electron impact energy was either 30 or 100 eV. The electron detector also consisted of two lens trains and two tandem hemispherical energy analyzers operated at about 0.080-eV resolution. The detector could be rotated around the scattering center to various fixed scattering angles on either side of the incoming electron beam. The electrons passing through the energy analyzer, which was set to transmit electrons with a specific energy ($E_0+2.25$ eV in the present study), were detected by an electron multiplier and counted using standard pulse counting and multichannel scaling (MCS) techniques.

The barium beam was generated by heating a tantalum crucible containing the naturally occurring isotopic mixture (71.7% ^{138}Ba, 11.3% ^{137}Ba, 7.8% ^{136}Ba, 6.6% ^{135}Ba, 2.4% ^{134}Ba, 0.1% ^{132}Ba, and 0.1% ^{130}Ba). The metal vapor effused from the crucible through a 0.5-cm-long 0.1-cm-diam tube and was further collimated by a 0.1-cm-diam aperture (in some cases with 6:1 but mostly with 30:1 collimation) to reduce the transverse Doppler width. The heater was a double strand resistor wire (to cancel the magnetic field generated by the current) which was surrounded by a grounded shield. It was wound directly on the crucible. Two layers of tungsten heat shield and a copper jacket surrounded the crucible. The Ba beam was placed on the rotation axis of the detector and it was perpendicular to the scattering plane. The beam density in the scattering region was typically 10^{12} cm^{-3} for the low collimation and about 10^{10}–10^{11} cm^{-3} for the high collimation case. The beam diameter in the scattering region was 1 mm in the latter case.

The laser system used for preparing the excited barium atoms consisted of an argon-ion laser and a tunable cw single-mode dye laser (Coherent Inc. Model 599-21 with Rhodamine 560 dye). Typical power level in the present experiments was about 5 mW with a few MHz width. The laser beam (diameter about 0.1 cm at the output coupler with a divergence 1.5 mrad) was located in the scattering plane at an angle θ_ν with respect to the incoming electron beam. The laser beam diameter at the scattering center was about 0.3 cm. The output of the laser was linearly polarized with polarization direction perpendicular to the scattering plane. This light beam was sent through a half-wave plate which was needed to control the angle of linear polarization with respect to the scattering plane (ψ). At zero electron scattering angle, the scattering plane is not defined. The incident electron beam and the laser beam, however, define a plane to which the laser polarization vector can be related. The laser beam then entered the vacuum chamber through an antireflection coated quartz window and after crossing the scattering region exited from the chamber through a similar window. The laser was tuned to excite only the $6s\,6p\ ^1P_1$ state of the ^{138}Ba ($I=0$) isotope. (See Fig. 1 for the energy-level diagram.) The notation of Ref. 11 is used here.

The optical pumping of the Ba resonance line at 5535 Å is somewhat complicated by the presence of a non-negligible branching ratio to the lower lying ^1D level. This branching ratio has been given[12] as 24:1 but recent measurements indicate that a 700:1 ratio is more likely.[13] Because of this uncertainty the dependence of the ^1P population as a function of branching ratio has been investigated in some detail. A plot of ^1S, ^1P, and ^1D population fractions versus branching ratio for typical experimental conditions (2 μsec pumping time, 5 mW laser power) is shown in Fig. 2. Based on this analysis and the observation that only weak electron scattering from the ^1D state has been observed in the present work, the 700:1 branching ratio seems to be the more accurate. Using this value, detailed calculations of population versus pumping time and laser power have been carried out. The effect of higher laser power is to drive the ^1S and ^1P populations to nearly equal values, whereas the pumping time allows more access to the ^1D level. Figure 3 demonstrates the population evolution versus pumping time for the conditions typical of this work. From this analysis it is estimated that approximately 30% of the beam is the ^1P excited state.

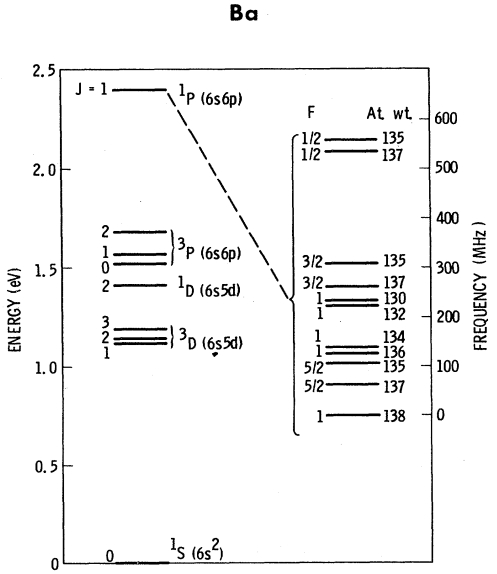

FIG. 1. Energy-level diagram for Ba. On the left side the electronic states of Ba are indicated up to 2.5 eV. On the right the hyperfine structure of the $6s\,6p\ ^1P$ state is shown with an expanded scale.

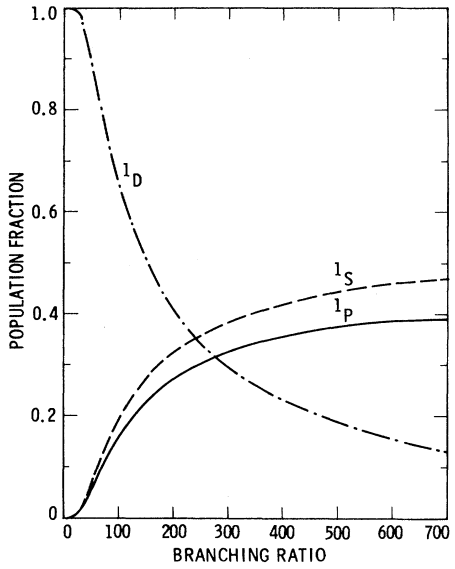

FIG. 2. Population fraction of the $6s^2\,{}^1S$, $6s6p\,{}^1P$, and $6s5d\,{}^1D$ states as a function of branching ratio for an illumination time of 2 μsec and pumping power of 5 mW (5×10^{-12} ergs cm^{-1} Hz^{-1}).

A schematic diagram of the scattering geometry is shown in Fig. 4. An enlarged diagram of the scattering region (made to proper scale) is shown in Fig. 5. For the present investigations the laser was always located in the scattering plane at either the $\theta_\nu=45°$ or 90° position. The scattering volume was defined by the intersection of the Ba beam, the laser beam, and the electron beam. It was about 0.1 cm in all three dimensions. The electron beam was adjusted to maximize the superelastic signal. Note that in the present investigation the Ba beam, the laser beam, and the electron beam were stationary and only the

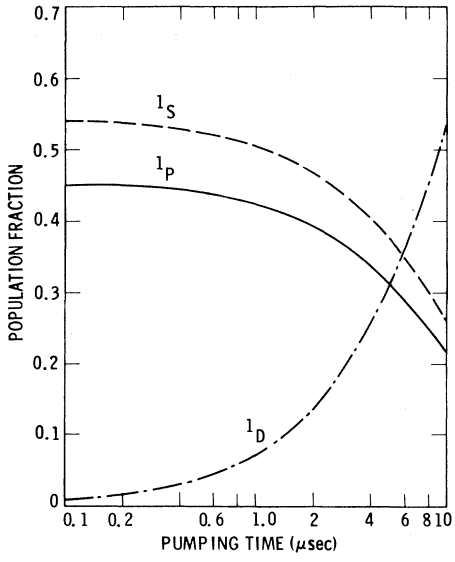

FIG. 3. Same as Fig. 2 except as a function of illumination time at fixed 700:1 branching ratio and 5 mW pumping power.

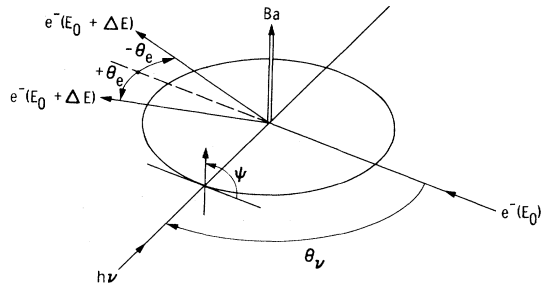

FIG. 4. Schematic representation of the scattering geometry. The Ba beam is perpendicular to the scattering plane. Laser beam is in the scattering plane at an angle θ_ν with respect to the incoming electron beam. Scattering to the left is associated with positive and to the right with negative scattering angles. Polarization of the light is rotated clockwise from the Ba target point of view and in the present experiments we start our measurements always at $\psi=90°$.

detector was moved. The detector view cone diameter at the scattering center was 0.37 cm (half angle 3.4°). The solid angle of signal collection was 3×10^{-4} sr for a scattering point located at the scattering center and decreased to 3×10^{-5} sr for the extreme edges of the scattering volume. The combination of the electron detector and source cones yielded an angular resolution of about $\pm1°$.

The superelastic scattering intensity I^S was measured as a function of ψ at fixed scattering angles ranging from $-15°$ to $+15°$. A switch on the half-wave—plate rotator initiated a 256-channel sweep in the MCS. A sweep corresponded to a rotation of the half-wave plate by 315° (a ψ rotation of 630°). The MCS then halted until the half-wave plate completed the 360° rotation and the switch initiated the next scan. This was repeated about 20 times at near-zero scattering angles and about 100 times for the 10° to 15° range.

III. RESULTS

Typical oscillatory curves representing the superelastic signal as a function of ψ for 100-eV impact energy and for

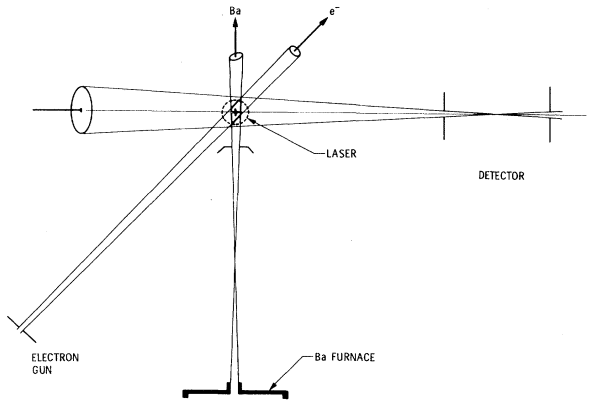

FIG. 5. Diagram showing the scattering region (drawn to proper scale). Intersection of the Ba, laser, and electron beams and the view cone are shown. Collimating apertures for the Ba beam and view cone are indicated.

several scattering angles with the laser located at $\theta_v=45°$ and 90° are shown in Figs. 6 and 7, respectively. The key points concerning these figures are (a) the oscillatory curves shift with scattering angle (b) at zero degree scattering angle the signal is maximum for $\psi=90°$ (Hertel and Stoll[2] found a minimum superelastic signal at $\psi=90°$ for Na) and (c) the signal at and very near $\theta_e=0°$ and at $\theta_e \geq 5°$ is symmetric in the sense that $I^S(\psi)=I^S(-\psi)$. However, at scattering angles between about 1° and 5° this symmetry is not found. A systematic study of this symmetry question was undertaken at 30- and 100-eV impact energies and at laser angles of 45° and 90° and the results are summarized in Figs. 8–10.

A theoretical expression for the superelastic intensity[4,5] which considers electron spin-orbit coupling in the Ba atom[9,10] for the present experimental arrangement can be given as[6]

$$I^S(\psi)_{E_0,\theta_e,\theta_v}=A+B\cos 2\psi \ . \tag{1}$$

This equation is based on and reflects the natural assumption of reflection symmetry of the scattering intensity with respect to the scattering plane:

$$I^S(\psi)=I^S(-\psi) \tag{2}$$

and is based on our knowledge that the interactions and the experimental conditions are symmetric with respect to reflection at the scattering plane. A and B are constants in the present consideration (they contain the source parameters) and depend on E_0,θ_e, and θ_v.

The observed asymmetry or equivalently the shift of the phase of $I^S(\psi)$ with scattering angle requires a modification of Eq. (1). The simplest empirical modification which describes the observation is

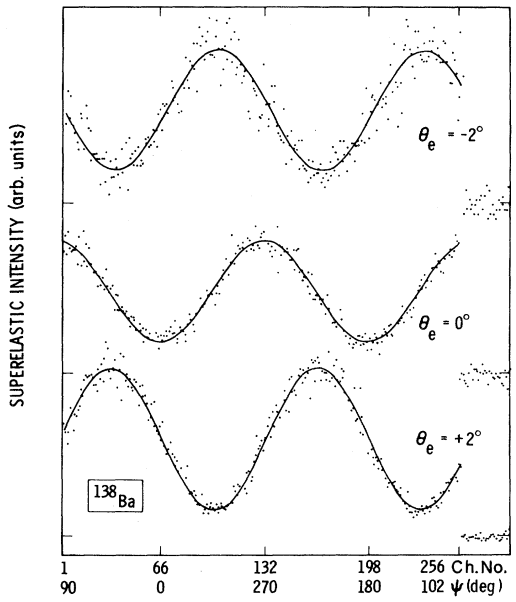

FIG. 6. Superelastic scattering intensities as a function of laser light linear polarization angle (ψ) and channel number of the multichannel scalar (ch. No.) at $E_0=100$ eV and θ_e ranging from −2° to +2°. Laser position corresponded to $\theta_v=45°$. Experimental points and a fit to them are indicated. Background signal is shown on the right side for each scattering angle.

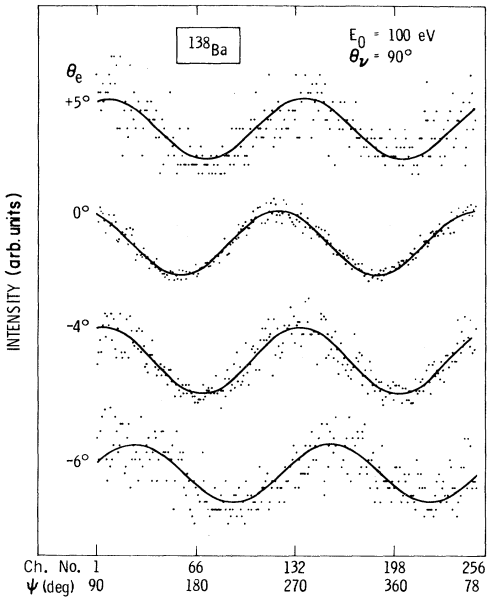

FIG. 7. Typical superelastic intensity curves for ^{138}Ba ($^1P_1$) obtained at 90° laser position, 100-eV electron impact energy, and +5° to −6° scattering angles as indicated as a function of laser polarization angle ψ. Equivalent channel numbers are also indicated.

$$I^S(\psi)_{E_0,\theta_e,\theta_v}=A+B\cos\{2[\psi+\alpha(\theta_e)]\} \tag{3}$$

or equivalently

$$I^S(\psi)_{E_0,\theta_e,\theta_v}=A+B'\cos 2\psi+B''\sin 2\psi \ . \tag{4}$$

Although Eqs. (3) and (4) were obtained empirically, identical equations are derived from theory if the reflection symmetry of the state created by the inverse collision process with respect to the scattering plane is not assumed.[6]

Figures 8–10 show that the $\alpha(\theta_e)$ function appears to be symmetric with respect to $\theta_e=0°$ for $\theta_v=90°$ cases and antisymmetric for $\theta_v=45°$ cases independently of impact energy. The rate of change of α with θ_e is, however, ener-

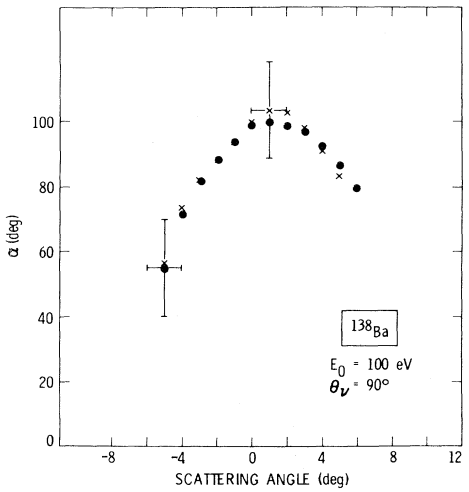

FIG. 8. Summary of shifts at $E_0=100$ eV, $\theta_v=90°$.

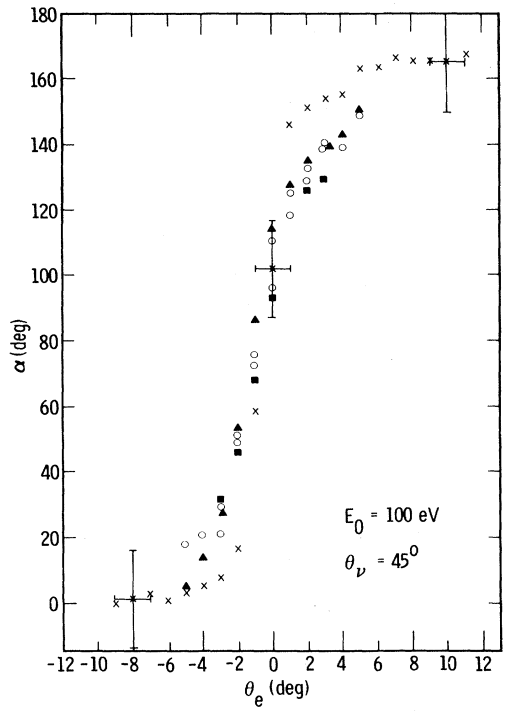

FIG. 9. Summary of shifts at $E_0=100$ eV, $\theta_\nu=45°$. Figure includes data points with and without externally applied magnetic field. Symbols ▲ and ■ represent data points obtained with a 15-mG magnetic field at the scattering region in the + and − direction of a coordinate line which is perpendicular to the electron beam and which is in the scattering plane.

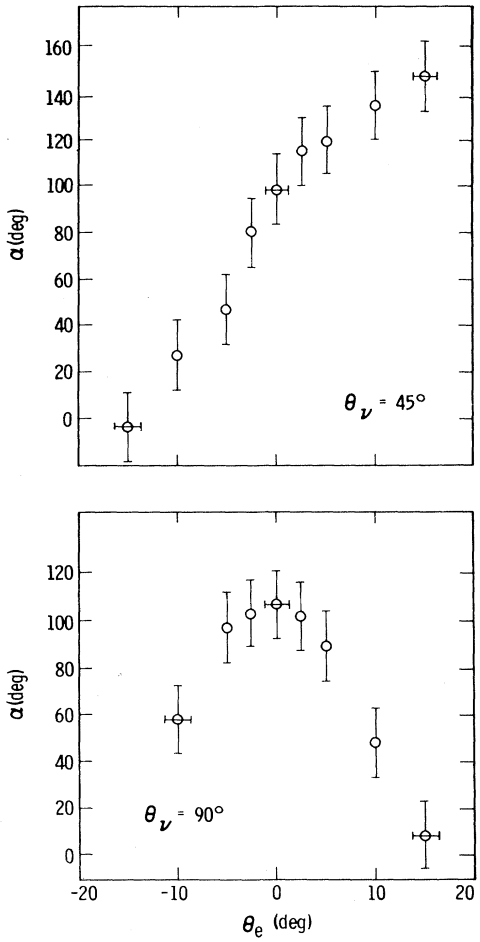

FIG. 10. Summary of shifts at $E_0=30$ eV, $\theta_\nu=45°$ and 90°.

gy dependent and is more pronounced at the higher impact energy. Within the experimental uncertainties, for both laser positions $\alpha(\theta_e=0°)=90°$ and $I^S(\psi=90°)$ is maximum. At around $\theta_e=\pm10°$, α becomes zero and the asymmetry disappears. It should be noted that in Eq. (4)

$$B'=\cos2\alpha \quad \text{and} \quad B''=-\sin2\alpha\ , \tag{5}$$

that is

$$\tan2\alpha=-\frac{B''}{B'}\ . \tag{6}$$

Since the observed asymmetry is unexpected and surprising, we undertook an extensive study to reconfirm this observation and to investigate the possible influence of various experimental conditions and parameters on this asymmetry.

IV. ADDITIONAL INVESTIGATIONS

A. Magnetic field

The presence of a magnetic field in the scattering region could lead to asymmetry in the scattering signal. In the present experiments, the magnetic field in the scattering region was reduced to about 1 mG under normal conditions. This was achieved by double μ-metal magnetic shielding, a pair of Helmholtz coils, and by the use of nonmagnetic materials in the scattering chamber. The pair of Helmholtz coils was needed to cancel a small magnetic field (5 mG) which leaks into the scattering chamber through the pumping ports. In order to ascertain whether magnetic field effects could play a role in the present observations, we repeated the experiments with magnetic fields of about 15 mG applied (by additional Helmholtz coils) both in the scattering plane and perpendicular to the scattering plane. These fields are not large enough to substantially perturb the electron trajectories but are an order of magnitude larger than the normal residual magnetic field in the scattering region. As a precautionary measure the polarity of the Helmholtz coils and of the dc heating coil on the Ba crucible was reversed for some of the studies.

The outcome of these investigations (at $E_0=100$ eV, $\theta_\nu=45°$) was negative in the sense that no change in the behavior of $I^S(\psi)$ and α with respect to θ_e was found. This is demonstrated in Fig. 11.

B. Laser beam alignment

The present experiments were designed and evaluated with the assumption that the pumping laser beam was in the scattering plane. Asymmetry may result from locating

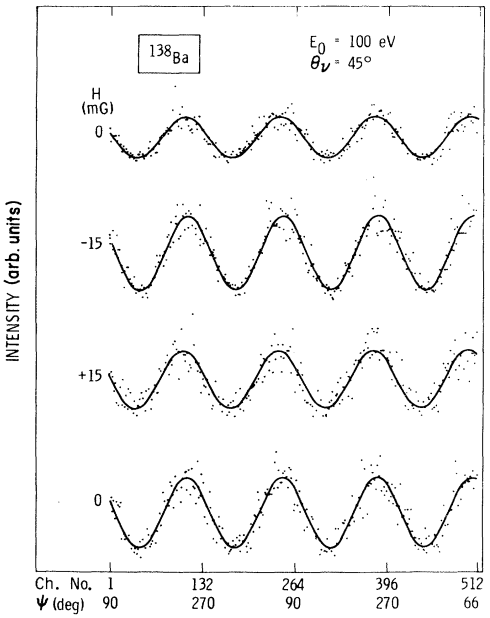

FIG. 11. Behavior of the superelastic scattering signal as a function of laser linear polarization (ψ) at 100-eV electron impact energy and 45° laser angle for zero and ±15-mG magnetic fields at the scattering center. θ_e was 2°.

the laser beam out of the scattering plane. From the mechanical construction of the system we estimated that the laser beam was aligned with this plane to within ±0.1°. This estimation was also confirmed by optical alignment checks. A collimated light beam was sent through the axis of the gun and the detector systems (at various detector angles). These beams illuminated a 0.1-cm-diam rod located with one end in the crucible and the other end protruding through the collimating aperture. This rod defined the Ba beam axis and the detector rotation axis. The point of illumination defined the scattering center and it remained stationary at all detector angles. The laser beam was then aimed at the scattering center and its inclination with the scattering plane was made zero.

To examine the possible effects of small deviations from the assumed laser beam geometry, we have tilted the laser beam above and below the scattering plane by 0.7° (the beam still crossing the scattering plane at the scattering center). For both offset geometries, we found no significant change in the behavior of $I^S(\psi)$ with respect to θ_e.

C. Polarization of laser beam

The investigations were carried out with the assumption that the dye laesr output was linearly polarized. If it were not, circular or elliptical polarization could cause asymmetric scattering. The source of elliptical polarization may be the laser itself or optical components (e.g., half-wave plate) between the laser and scattering center. Several measurements were made to see whether elliptical polarization might influence the observations.

The polarization characteristics of the dye laser were determined by measuring the laser beam intensity passing through a Glan-Thompson prism with its polarization direction parallel ($I_{||}$) and perpendicular ($I_\perp$) to the primary laser polarization direction (vertical). The beam intensity passing through the prism was measured with a photodiode. Calibrated neutral density filters were used to reduce the $I_{||}$ value to the $I_\perp$ value, and it was found that 99.4% of the total laser beam intensity corresponded to $I_{||}$ and 0.6% to $I_\perp$. This indicates that the laser beam is very nearly linearly polarized. (The major and minor axes for the polarization ellipse have the ratio 99.4 to 0.6.) This situation can be further improved by a factor of 10^4 by sending the laser beam through a stationary Glan-Thompson prism with its transmission direction parallel to the laser light polarization before it reaches the half-wave plate. This was done in several of our experiments. It was also found that the light transmitted by the half-wave plate retained the same ellipticity as the light illuminating the half-wave plate. This means that no ellipticity was introduced by the half-wave plate.

In one study, a Glan-Thompson prism was placed between the half-wave plate and the scattering center and the $I(\psi)$ vs ψ measurements were repeated at the various scattering angles. The prism had an extinction ratio of 10^{-4} and its polarization direction was chosen such that the combined half-wave plate and prism system yielded maximum transmission. Since the half-wave plate rotates the linear polarization with twice the angular frequency of its own rotation, we rotated the Glan-Thompson prism twice as fast as the half-wave plate. This assured that the polarization directions for the half-wave plate and the Glan-Thompson prism remained in phase and at the maximum transmittency of these two combined elements. Since the beam exiting from the Glan-Thompson prism is slightly offset with respect to the entering beam, the pumping laser beam described a small circle at the scattering region (the center of this circle being defined by the original direction of the laser beam before the prism). This effect superimposed a small modulation on the normal oscillation of $I^S(\psi)$ and the consecutive peaks did not have exactly the same magnitude. This effect, however, does not influence our conclusions concerning the behavior of α, and again it was found that the general behavior of α with respect to θ_e remained the same when the experiments were performed with or without the Glan-Thompson prism.

In some of our earliest measurements uncertainty was introduced into our determination of the value of α by the uncertainty (about ±10°) in the pumping light beam polarization at the beginning of the MCS scan (corresponding to the first channel). A more accurate calibration of ψ with respect to the first channel was made subsequently and the system has been adjusted such that the first channel signal corresponded to $\psi = 90° \pm 2°$ (polarization is vertical). The setup for this calibration is shown in Fig. 12. The half-wave plate was rotated to cause the rotation of the linear polarization of the light beam. A linear polarizer with its polarization vector horizontal (in the plane of Fig. 12) was placed between the exit window of the vacuum chamber and the photodiode. The half-wave plate was then rotated and the MCS actuating switch was adjusted to set channel 1 to correspond to minimum signal in the photodiode. (The signal was converted to counts for the

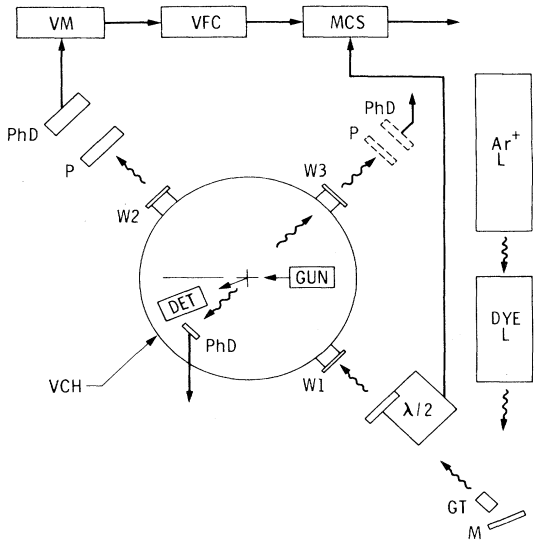

FIG. 12. Experimental arrangement for the characterization of pumping and fluorescence light beams and for the calibration of laser polarization in terms of channel number of the MCS. The symbols have the following meaning: *L*, laser; *M*, front surface coated minor; GT, Glan-Thompson prism; $\frac{1}{2}$, half-wave plate and rotator; *W*, window; VCH, vacuum chamber; GUN, electron gun; DET, electron detector; *P*, linear polarizer; PhD, photodiode; VM, volt meter and amplifier; VFC, voltage to frequency converter. Initial laser polarization was perpendicular to the scattering plane.

MCS by a voltage to frequency converter.) A typical scan (signal versus channel number) is shown in Fig. 13. By this procedure we calibrated ψ with an accuracy of about $\pm 2°$. In addition to the uncertainty in ψ, there is an uncertainty in θ_e which has to be considered for the uncertainty of the $\alpha(\theta_e)$ function. This question is further discussed below in Sec. IV F.

D. Laser beam intensity

Under normal operating conditions the laser beam intensity was about 5 mW (cw single mode). This corresponds to about 1.5×10^{16} photons/sec or to 5×10^{-12} ergs cm^{-3} Hz^{-1}, and produces a power broadening of about 27 MHz. This broadening when combined with the natural linewidth and with the Doppler broadening could, in principle, cause overlap and mixing of the hyperfine levels and therefore influence the superelastic scattering. As we shall see below (Sec. IV G) this does not affect our experiments. To further assure ourselves, we reduce the laser beam intensity by about a factor of 10 in steps with the application of neutral density filters, and reinvestigated the dependence of $I^S(\psi)$ and α at these reduced intensities. No significant change compared to the normal power density was found.

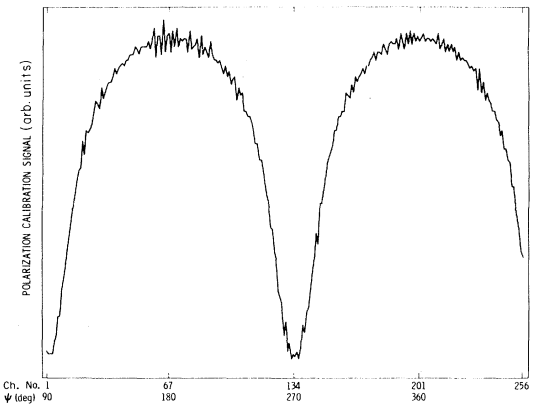

FIG. 13. Calibration curve for photodiode signal vs channel number. Zero signal corresponds to $\psi=90°$. (For experimental arrangements see Fig. 12.)

E. Barium beam density and collimation

The Ba beam density and collimation affects the radiation trapping (depolarization) and Doppler width, respectively. The asymmetry was first noticed with a beam collimation of 6:1. Subsequent experiments were carried out with a 30:1 collimation which corresponds to a Doppler broadening of about 36 MHz (FWHM). With this collimation the typical beam density in the scattering region is estimated to be about 10^{10}–10^{11} cm^{-3}. The superelastic scattering experiments were repeated several times at lower beam densities by gradually decreasing the heater current. Judging on the basis of the signal, we estimate that the beam density was lowered to about 10^9 cm^{-3} for some of the measurements. In all these experiments, however, the same asymmetry was found, indicating that radiation trapping or Doppler broadening plays no role in this asymmetry. Another check on the influence of beam density concerns the change of maximum to minimum superelastic scattering density ratio in the $I^S(\psi)$ modulation with ψ. When we increased the beam density to about 10^{13} cm^{-3} the modulation disappeared due to radiation trapping (and consequent depolarization). As we lowered the beam density the modulation depth increased and then leveled at around $I_{\max}/I_{\min}=0.9$ in the case of $E_0=100$ eV, $\theta_e=5°$,$\theta_e=45°$.

F. Angular and energy resolution and scale calibration

The angular resolution selected in the present measurement was dictated by a compromise between high signal level and high angular resolution requirements. Some measurements were carried out with $\pm 2°$ but most of them with $\pm 1°$ angular resolution in the electron detector. Because the phase, α, which is associated with the asymmetry of the superelastic signal, changes very rapidly with scattering angle at low θ_e values, one would desire very good angular resolution. This can only be achieved with sacrifice in signal intensity. We compromised on $\pm 1°$.

The question of angular calibration and of associated angular error is crucial for the present experiments because of the rapid variation of α with θ_e. During several years of experience we found that mechanical and optical alignment of the gun and detector is not sufficient in determining the true zero scattering angle. The electron beam, due to surface and various field effects, may not follow the exact mechanical axis. It is more reliable to determine the actual zero scattering angle (and therefore

the angular scale) by measuring the symmetry of an inelastic, strongly forward-peaking scattering signal around the nominal zero degree point. Usually there is some problem with this signal at zero angle due to interference from the direct beam which, however, disappears in our case at about $\pm 0.5°$. The accuracy to which the true zero angle can be determined by this procedure is $\pm 1°$. This uncertainty of 1° results in an uncertainty in the $\alpha(\theta_e)$ function (including the $\pm 2°$ uncertainty in measuring ψ itself) of about 15°.

The finite size of the detector view cone (in combination with the electron beam divergence) generates an uncertainty in the scattering angle and in the definition of the scattering plane. In any real experiment there is not a unique scattering plane but a distribution of scattering planes. In the present experiments the tilt angle of these planes with respect to the laser beam is of some concern as discussed in Sec. IV B above. More important, however, is, that the definition of the scattering plane is not meaningful at scattering angles smaller than the angular divergence of the incoming and detected electron beam cones.

Energy resolution was not a major concern in the present measurements (the nearest superelastic feature is 0.6 eV away); however, good collimation of the incoming electron beam was important. A wide beam divergence can cause serious background problems at low angles (a few degrees) where the superelastic signal falls off very fast with increasing θ_e. To form a well-collimated beam, we utilized a double hemispherical gun but operated it at a low energy resolution (80 mV). There was no need in the present experiments to calibrate the electron impact energy scale. The few tenths of an eV uncertainty has no consequence for the present work.

G. Fluorescence intensity

The fluorescence signal represents a convenient means for monitoring the laser pumping process.[14] In the present case a photodiode was mounted in the scattering plane at 90° with respect to the laser beam direction (Fig. 12) to measure the fluorescence intensity (I^f) as a function of the laser light polarization angle (ψ) with respect to the scattering plane. Figure 14 shows this signal as a function of ψ or equivalently as the MCS channel number. The fluorescence signal corresponded to the expected dipole radiation, given for our case as

$$\frac{dI^f}{d\Omega}(\psi)=\frac{C}{\Gamma}\cos^2\gamma\cos^2\gamma' , \tag{7a}$$

where $\gamma=-\psi(\pi/2)$, and γ' is the polarization direction for the detector (measured with respect to the vertical direction), Γ is the spontaneous decay rate, and C contains the atomic density, dipole matrix element, energy density of pumping beam, and atomic constants.[15] For a detector without a polarization preference

$$\frac{dI^f}{d\Omega}(\psi)\propto\cos^2\gamma=\cos^2(\psi-90°). \tag{7b}$$

The fluorescence signal was found to be maximum when γ was 0° ($\psi=270°$) and minimum (residual signal is due to scattered light) at $\gamma=90°$ ($\psi=0°$). The unpolarized fluorescence signal as a function of ψ (Fig. 14) satisfies the condition $I^f(\psi)=I^f(-\psi)$. *This study shows that the pumping and fluorescence mechanism is as expected and that the asymmetry is associated with the collision process.*

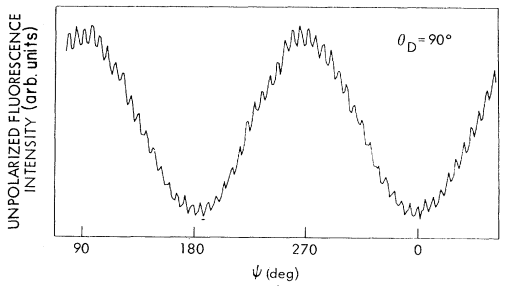

FIG. 14. Unpolarized fluorescence intensity as a function of pumping light polarization angle (ψ). Photodiode detector was located at 90° with respect to the laser beam. [At $\psi=0°$ and 180°, the polarization vector of the pumping laser beam ($\vec{E}_p$) is in the plane defined by the laser and detector directions.]

H. The hyperfine spectrum

In order to assess the degree to which isotopes other than ^{138}Ba may contribute to or interfere with the observations, we swept the dye laser wavelength and generated hyperfine spectra in both the fluorescence and the superelastic channels.

Figure 15 shows the fluorescence spectrum. The dominant feature corresponds to radiation by ^{138}Ba. There is definite indication for 137 and 135 isotopes at around 63 and 105 MHz, respectively (with respect to the ^{138}Ba feature). The frequency values corresponding to the various hyperfine levels were taken from Refs. 16–18. The FWHM of the ^{138}Ba feature was found to be about 51 MHz. This compares well with the 50-MHz width calculated from the 19-MHz natural width, the 5-MHz laser width, and the Doppler and power broadening under our experimental conditions (36 and 27 MHz, respectively). The contribution to the fluorescence signal from isotopes other than ^{138}Ba when the pumping occurs with a laser frequency which corresponds to zero on the scale of Fig.

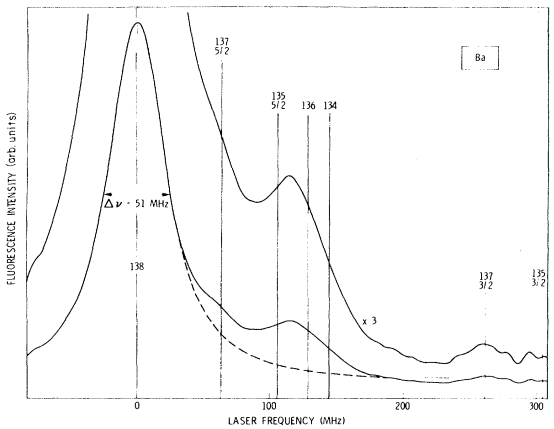

FIG. 15. Hyperfine spectrum in the fluorescence channel. Frequency values for the various isotopes and F values are indicated. $\theta_v=90°, \psi=90°$.

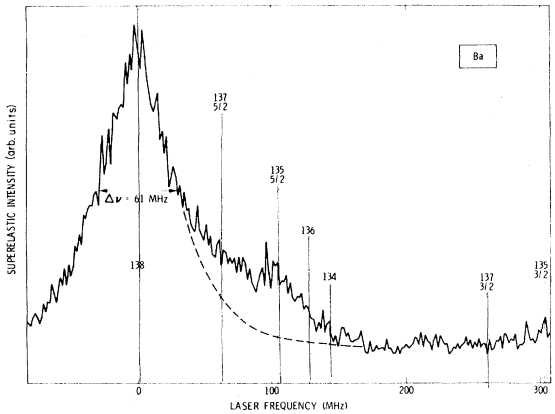

FIG. 16. Hyperfine spectrum obtained in the superelastic channel. Frequency values for the various isotopes and F values are indicated. $E_0=100$ eV, $\theta_e=2°$, $\theta_\gamma=90°$, and $\psi=90°$.

14 is negligible. It should be noted, however, that the laser polarization was chosen as $\psi=90°$ for this spectrum, which represents the optimum fluorescence condition for the even Ba isotopes. (At $\psi=0°$ the fluorescence from the even Ba isotopes is zero if we neglect the effect of finite solid angle of detection. Fluorescence due to the odd Ba isotopes is more complicated to describe and it does not vanish at any value of ψ.) This spectrum gives us information on the laser pumping conditions and is consistent with our expectations.

The spectrum generated in the superelastic electron scattering channel is shown in Fig. 16. It is very similar to the fluorescence spectrum. There is a slight additional broadening due to the electron energy resolution. In this spectrum the ^{138}Ba linewidth is 61 MHz (FWHM). The ^{138}Ba signal is by far the dominant feature. Under our normal experimental conditions, when the pumping occurs at the frequency corresponding to the peak of the ^{138}Ba signal, the contributions to $I^S(\psi)$ from other than the 138 isotope are completely negligible. Again, it should be noted that the polarization in Fig. 16 was chosen to give maximum signal for the 138 peak. The behavior of the superelastic signal associated with the other isotopes is not known and the situation will be different at other values of ψ. On the basis of the level widths and separations and of the isotopic ratios, we can conclude that contribution to the ^{138}Ba superelastic signal from other isotopic species will be small under our experimental conditions at any value of ψ. Furthermore, even if significant contributions to $I^S(\psi)$ from odd isotopes did exist at certain values of ψ, this alone would not explain the observed asymmetry for the following two reasons: (a) in addition to mixing in odd parity states it would also be required that these states be oriented in order to explain the observed asymmetry and (b) the Percival-Seaton hypothesis of decoupling of the nuclear spin in electron scattering should hold very well and therefore nuclear spin does not enter the scattering interaction except in the statistical sense.

V. SUMMARY AND CONCLUSIONS

Owing to the very systematic nature of the data that has been accumulated over the past three years, two possible conclusions must be considered: (1) the results are an artifact of the experimental conditions, which we cannot recognize at present, or (2) an effect has been observed which is inconsistent with our present understanding of collision physics for heavy atoms.

In the former category, the checks which have been performed are certainly more rigorous than usual for electron-atom collision experiments. This implies that either there is an unknown systematic error which we are unable to discover, or that the sensitivity of these experiments to even μsr misalignments makes this approach essentially useless. Since a number of electron-photon coincidence experiments with heavy atoms (e.g., mercury) have been reported, this possibility should apply with some validity to those data also. A more probable explanation is that the experimental observation pertains to an ensemble of atomic species, while the theoretical considerations refer to individual atoms or to an ensemble of identical species.

If, however, reflection invariance is violated in these experiments then some modifications to our understanding of fundamental atomic processes for heavy atoms must be made. At this time we do not support a strong claim to this and would be willing to accept a less dramatic conclusion.

ACKNOWLEDGMENTS

We would like to express our gratitude to I. Hertel and P. Farago for valuable discussions concerning the present work. This work was supported by the National Aeronautics and Space Administration, Contract No. NAS-7-100 and by the National Science Foundation, Research Grant No. PHY-79-05971.

*Present address: Phillips Petroleum Co., Bartlesville, OK 74004.

†Present address: University of California, Los Alamos National Laboratory, P. O. Box 1663, Los Alamos, NM 87545.

‡Deceased.

[1]K. Blum and H. Kleinpoppen, Phys. Rep. 52, 203 (1979).

[2]I. V. Hertel and W. Stoll, Adv. At. Mol. Phys. 13, 113 (1977).

[3](a) S. W. Jensen, Ph. D. thesis, University of California, Riverside, California, 1978 (unpublished). (b) D. F. Register, S. Trajmar, S. W. Jensen, and R. T. Poe, in *Coherence and Correlations in Atomic Collisions,* edited by H. Kleinpoppen and J. F. Williams (Plenum, New York, 1980). (c) D. F. Register and S. Trajmar, International Symposium on Correlation and Polarization in Electron Atom Collisions, July 1981, National Bureau of Standards, Gaithersburg, Maryland (unpublished).

[4]J. Macek and I. V. Hertel, J. Phys. B 7, 2173 (1974).

[5]U. Fano and J. H. Macek, Rev. Mod. Phys 45, 553 (1973).

[6]Gy. Csanak, D. F. Register, and S. Trajmar (unpublished).

[7]H. W. Hermann, I. V. Hertel, W. Reiland, A. Stamatovic, and W. Stoll, J. Phys. B 10, 251 (1977).

[8]I. C. Percival and M. S. Seaton, Philos. Trans. R. Soc. London, Ser. A 251, 113 (1958).

[9]K. Blum, F. J. da Paixâo, and Gy. Csanak, J. Phys. B 13, L257 (1980).

[10]F. J. da Paixâo, N. T. Padial, Gy. Csanak, and K. Blum, Phys.

Rev. Lett. 45, 1164 (1980).
[11]C. E. Moore, National Bureau of Standards Circular No. 467 (U.S. GPO, Washington, D.C., 1952).
[12]B. M. Miles and W. L. Wiese, National Bureau of Standards Technical Note No. 474 (U.S. GPO, Washington, D.C., 1969).
[13]A. F. Bernhardt, D. E. Duerre, J. R. Simpson, and L. L. Wood, J. Opt. Soc. Am. 66, 416 (1976).
[14]A. Fisher and I. V. Hertel, Z. Phys. A 304, 103 (1982).
[15]A. Corney, *Atomic and Laser Spectroscopy* (Clarendon, Oxford, 1977), pp. 530–512.
[16]A. F. Bernhardt, D. E. Duerre, J. R. Simpson, and L. L. Wood, Opt. Commun. 16, 166 (1976).
[17]G. Nowicki, K. Bekk, S. Goring, A. Homser, H. Rebel, and G. Schatz, Phys. Rev. C 18, 2369 (1978).
[18]P. E. G. Baird, R. J. Brambley, K. Burnett, D. N. Stacey, D. M. Warrington, and G. K. Woodgate, Proc. R. Soc. London 365, 567 (1979).